

Article

# On Phase and Amplitude Extraction in Bichromatic Ionization: A Proposal

Maria M. Popova <sup>1,2,3,\*</sup> , Alexei N. Grum-Grzhimailo <sup>2</sup> and Elena V. Gryzlova <sup>2,3,\*</sup> 

<sup>1</sup> Faculty of Physics, Lomonosov Moscow State University, 119991 Moscow, Russia

<sup>2</sup> Skobeltsyn Institute of Nuclear Physics, Lomonosov Moscow State University, 119991 Moscow, Russia

<sup>3</sup> A.V. Gaponov-Grekhov Institute of Applied Physics, Russian Academy of Sciences, 603950 Nizhny Novgorod, Russia

\* Correspondence: mm.popova@physics.msu.ru (M.M.P.); gryzlovaev@depni.sinp.msu.ru (E.V.G.)

**Abstract:** In the paper we propose a method for characterizing VUV pulse(s) in a bichromatic ionization setup. The scheme is based on s-shell ionization by joint action of circularly polarized fundamental harmonic and linearly polarized second one. The advantage of the proposed approach is the existence of kinematic (geometrical) zeros of partial amplitudes which positions can be extracted with minimal number of theoretical (spectroscopic) assumptions and therefore they may serve as natural reference points in measuring the relative phase and amplitude of the harmonics. In the paper, we investigate a general possible geometry setup with more detailed consideration of the edge cases and present calculation and numerical stimulation for helium ionization as an illustrative example.

**Keywords:** photoionization; bichromatic field; coherent control; s-shell; variationally stable method; helium (to ten)

## 1. Introduction

A two-photon absorption remains the simplest species in the zoo of non-linear processes induced by an electromagnetic field in matter since such possibility was first supposed [1]. A resonant two-photon ionization allows to reveal the temporal structure of a light beam because it is much more sensitive to the phase, duration and coherency than a single-photon ionization. The combination of resonant and non-resonant ionization is even more promising because the non-resonant pathway may serve as a reference point for resonant one giving rise an additional phase between scattering (intrinsic) and dynamical (imposed by the field) phases.

Interference between different multi-photon pathways was used as a tool for diagnostic of a field in a variety of different setups. Since a constant phase is crucial to the interference, setups based on a one seeding frequency and its multiple harmonics are widely applied. Implementation of Free-Electron-Laser (FEL) and High Harmonic Generation (HHG) [2–6] facilities enabling generation of a phase-locked harmonics in vacuum ultra violet (VUV) range made it possible to observe interference effects in high energy domain [7]. While RABBITT (reconstruction of attosecond beating by interference of two-photon transitions) scheme is widely used to characterize VUV pulse(s) with attosecond precision [8–10], the bi-harmonic setup that has its own drawbacks and benefits was applied for the same purpose very few times [11,12]. Here we consider the bi-chromatic ionization i.e., the processes caused by  $(n\omega + m\omega)$  field with a different combination of  $n, m$ :

$$A + \left\{ \begin{array}{c} \hbar(m\omega) + \dots + \hbar(m\omega) \\ \hbar(n\omega) \end{array} \right\} \rightarrow A^+ + e^- . \quad (1)$$

Photoemission probability caused by the bichromatic ionization (1) as a function of emission direction oscillates with the phase between harmonics. Two different setups



**Citation:** Popova, M.M.; Grum-Grzhimailo, A.N.; Gryzlova, E.V. On Phase and Amplitude Extraction in Bichromatic Ionization: A Proposal. *Photonics* **2023**, *10*, 1069. <https://doi.org/10.3390/photonics10101069>

Received: 27 August 2023  
Revised: 11 September 2023  
Accepted: 14 September 2023  
Published: 22 September 2023



**Copyright:** © 2023 by the authors. Licensee MDPI, Basel, Switzerland. This article is an open access article distributed under the terms and conditions of the Creative Commons Attribution (CC BY) license (<https://creativecommons.org/licenses/by/4.0/>).

may be applied for measuring: several detectors placed at different angles which allow to reconstruct an angular distribution at fixed phase, or one detector registering the signal as a function of phase offset allows to extract some system details such as a scattering phase in different channels. These and similar combinations of frequencies have been applied in optical domain to manipulate electron vortices [13], to exploit HHG with different polarization [14–19], to create field with chirality [20–22], to realize RABBITT in strong field multi-photon regime [23,24].

Generally, the theoretical methods developed to describe a bichromatic ionization such as perturbation theory, strong field approximation (SFA) [25–27], and direct solution of time-dependent Schrödinger equation (TDSE) [28,29] may be implemented in VUV domain too [30,31]. Nevertheless, in the VUV domain the perturbation theory is applied more often because the Keldysh parameter is higher.

The bichromatic scheme has been actively explored for atoms [32–35], molecules [20,36–38], and even solids [39,40], but the experiments with atoms has an advantage because of the initial spherical symmetry. Within the dipole approximation, if the interference occurs between transitions involving odd (even) number of photons, it appears in the integral cross section, and if it occurs between odd and even number of photons, then it can be traced only in the differential parameters, for example, the photoelectron angular distribution and spin polarization [41]. To this end, atomic samples provide a valuable benchmark for understanding more complex systems. In order to violate the spherical symmetry, an additional field may be applied [42,43].

An important feature of the bichromatic ionization is that a particular channel can be emphasized or suppressed by adjustment photon energy to a resonance. The role of autoionization in coherent control over photoelectron emission was discussed in [44–46].

One of the obstacles for applying the bichromatic scheme to characterize a FEL radiation is that it possesses a lower longitudinal coherency than the HHG facilities, and, furthermore, there is an additional fraction of incoherent radiation. As a result, matching of two-photon and single-photon signals aimed to maximize the interference works not as good as wanted. As a result, some additional assumptions may be needed. For example, in recent work [47], the photoemission from helium was set to be constant to calibrate the photoemission from neon. Here we propose a scheme which allows to clearly distinguish between the single-photon and multi-photon channels, between the pulse and spectroscopic phases and measure an incoherent fraction. The scheme works like a sundial: the circularly polarized fundamental harmonic causing two-photon transitions forms a clock-ticks and the second harmonic causing singlephoton transitions works as a gnomon and indicates a phase between harmonics (Figure 1). Moreover, as discussed in Section 6, the scheme is also applicable to circularly polarized fundamental harmonic causing  $n$ -photon transitions and linearly polarized  $n$ -order harmonic.

Because our goal is to minimize number of involved theoretical (spectroscopic) assumptions, we consider ionization of  $s$ -shell neglecting a target fine-structure and we chose helium in the ground state as illustrative target. This target has been a subject of a bunch of investigations. The relatively general geometry, i.e., elliptically polarized radiation with accounting of non-dipole terms was discussed in [48,49]. A very general setup with arbitrary polarization and mutual directions of harmonics for any possible target was presented by ours in [50]. Here we want to focus on the benefits which geometries with circularly polarized fundamental and linearly polarized second (multiple) harmonics provide.

The technique of pulse generation and photocurrent detection is progressing, and in the near future, it is reasonable to expect that an any particular geometry will be available.

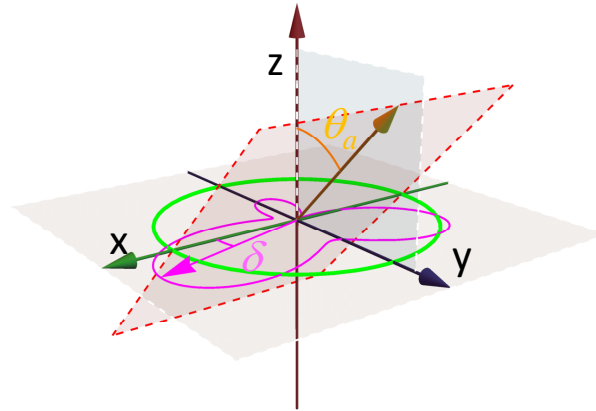


**Figure 1.** The proposed geometry: circularly polarized fundamental harmonic (green line), linearly polarized in the direction  $\{\theta_a\}$  second (multiple) harmonic (orange arrow), and a schematic way to define the phase between harmonics (magenta line).

### 2. Theoretical Model

Supposing the infinite long pulse, we take the electric field in a form

$$E_{\omega+2\omega}(t) = E_{\omega}e_{\omega}e^{-i\omega t} + E_{2\omega}e_{2\omega}e^{-i(2\omega t+\phi)}, \tag{2}$$

where  $E_{\omega}$  and  $E_{2\omega}$  are the amplitudes of the  $\omega$  and  $2\omega$  components,  $\phi$  is their phase difference,  $e_{\omega} = e_+ = -(e_x + ie_y)/\sqrt{2}$  and  $e_{2\omega} = \cos\theta_a e_z + \sin\theta_a(\cos\phi_p e_x + \sin\phi_p e_y)$  are the unit vectors of their polarization, i.e.,  $\omega$  component is right circularly polarized and  $2\omega$  component is linearly polarized in the direction  $\{\theta_a, \phi_a\}$  in a chosen coordinate system. In the considered geometry the phase is a doubled angle between  $\omega$  electric strength and projection of the  $2\omega$  electric strength to  $xy$ -plane at the moment when amplitude of the second is maximal.

Following the approach described in [50], the corresponding photon statistical tensor  $\rho_{kq}^{\gamma}$  is presented in a form:

$$\rho_{kq}^{\gamma} = \rho_{kq}^{2\omega,2\omega} + \rho_{kq}^{\omega+\omega,\omega+\omega} + \left( \rho_{kq}^{\omega+\omega,2\omega} + \rho_{kq}^{2\omega,\omega+\omega} \right), \tag{3}$$

where the term  $\rho_{kq}^{2\omega,2\omega}$  is associated with the absorption of a photon with energy  $2\omega$

$$\rho_{kq}^{2\omega,2\omega} = \sum_{\lambda,\lambda'=0,\pm 1} c_{\lambda}c_{\lambda'}(-1)^{1-\lambda'}(1\lambda,1-\lambda'|kq), \tag{4}$$

where  $c_0 = \cos\theta_a$  and  $c_{\pm} = \mp \sin\theta_a(\cos\phi_p \mp i \sin\phi_p)/2$ , and the standard notation for the Clebsch–Gordan coefficients is used; the term originating from the absorption of two photons with energy  $\omega$

$$\rho_{kq}^{\omega+\omega,\omega+\omega} = (22,2-2|k0), \tag{5}$$

and their interference ( $2\omega + \omega$ )

$$\rho_{kq}^{\omega+\omega,2\omega} = \sum_{\lambda=0,\pm 1} c_{\lambda}(-1)^{1-\lambda}(22,1-\lambda|kq), \quad \rho_{kq}^{2\omega,\omega+\omega} = \sum_{\lambda=0,\pm 1} c_{\lambda}^*(1\lambda,2-2|kq). \tag{6}$$

The permutation equation for the interference term is  $\rho_{kq}^{\omega+\omega,2\omega} = (-1)^{(1+q)}\rho_{k-q}^{*2\omega,\omega+\omega}$ .

When an experiment is aimed to characterize a pulse, it is natural to choose a system with minimal possible number of reaction channels. One of best choices is an  $s$ -shell ionization of noble gases. For these targets orbital moments of an emitted electron and

a final system are equal and determined by number of absorbed photons and their polarization. Besides, a target supposed to be light in order to neglect the fine-structure interaction. Therefore, we may characterize a final state with only one quantum number i.e., photoelectron angular momentum  $l$ .

According to the angular momentum theory [51], the photoelectron angular distribution (PAD) may be obtained by convolution of the statistical tensor of the system with the corresponding efficiency tensor:

$$W = \text{Tr}[\rho(l, l')\varepsilon(l, l')^*] \equiv \sum_{kq} \rho_{kq}(l, l')\varepsilon_{kq}(l, l')^*. \tag{7}$$

Further following the approach [50], in the single-electron approximation for  $s$ -shell ionization we cast photoelectron angular distribution in a very simple form:

$$W(\vartheta, \varphi) = \frac{1}{4\pi} \sum_{kqnn'l'l'} (-1)^l (l0, l'0 | k0) \rho_{kq}^\gamma(l, l') \frac{\sqrt{4\pi}}{\hat{k}} Y_{kq}(\vartheta, \varphi) A_l^{(n)} A_{l'}^{(n')*}, \tag{8}$$

where  $\hat{k} = \sqrt{2k+1}$ ,  $Y_{kq}(\vartheta, \varphi)$  denotes the spherical harmonic as function of an electron emission angle, and  $A_l^{(n)}$  is the  $n$ -th order reduced transition amplitude for the electron with momentum  $l$ . It should be emphasized for the reason of clearness that  $A_l^{(2)}$  indeed is a second order reduced transition amplitude of two dipole photon absorption. It can be composed from two first order amplitudes by the use of Formula (A.63) from [51]. More details are presented in Section 4.

The PAD (8) may be splitted as:

$$W(\vartheta, \varphi) = W^{(\omega)}(\vartheta, \varphi) + W^{(2\omega)}(\vartheta, \varphi) + W^{(\omega, 2\omega)}(\vartheta, \varphi); \tag{9}$$

where the contribution of two-photon ionization by circularly polarized fundamental harmonic:

$$W^\omega(\vartheta, \varphi) = \frac{1}{4\pi} \frac{3}{8} |A_{\varepsilon d}^{(2)}|^2 \sin^4 \vartheta; \tag{10}$$

the contribution of single-photon ionization by linearly polarized second harmonic:

$$W^{2\omega}(\vartheta, \varphi) = \frac{1}{4\pi} |A_{\varepsilon p}^{(1)}|^2 (\cos \theta_a \cos(\vartheta) + \sin \theta_a \sin \vartheta \cos(\phi_p - \varphi))^2; \tag{11}$$

and, finally, the interference term:

$$W^{(\omega, 2\omega)}(\vartheta, \varphi) = \frac{1}{4\pi} \sqrt{\frac{3}{2}} |A_{\varepsilon p}^{(1)} A_{\varepsilon d}^{(2)*}| \sin^2 \vartheta \times (\cos(\theta_a) \cos(\vartheta) + \sin \theta_a \sin \vartheta \cos(\phi_a - \varphi)) \cos(2\varphi - \delta). \tag{12}$$

Notice that  $\cos(\theta_a) \cos(\vartheta) + \sin \theta_a \sin \vartheta \cos(\phi_p - \varphi)$  is a simple cosine of the angle between the polarization vector of second harmonic and photoelectron emission angle. The phase  $\delta$  is defined by the scattering phase  $\sigma$  in the  $p$ - and  $d$ -channels and the phase between harmonics  $\phi$ :  $\delta = \sigma_p - \sigma_d - \phi$ .

The PADs produced by the fundamental (10) and the second (11) harmonics are axially symmetric with respect to the propagation direction and polarization vector, correspondingly. If the axes of symmetry coincide ( $\theta_a = 0$ ), the incoherent sum of Equations (10) and (11) is symmetrical too, nevertheless the contribution of the interference term (12) does not possess axial symmetry at any  $\{\theta_a, \phi_a\}$ . Two features of the interference contribution may be deduced from (12): (a) there are two planes of zero contribution ( $\varphi = \delta/2 \pm \pi/4$ ) which rotate with phase shift between harmonics; (b) there is one plane of zero contribution

$(\cos(\theta_a)\cos(\vartheta) + \sin\theta_a\sin\vartheta\cos(\phi_p - \varphi) = 0)$  which stay steady at phase shift changing and is determined only by the geometrical setup.

### 3. Discussion of the Geometry Setup

In this section we discuss two geometrical setups which allow to use the zeros of (10)–(12) to clearly distinguish the coherent and incoherent contributions with minimal amount of detectors and spectroscopic data. For example, in [12] at least two complex ratios of amplitudes are supposed to be known from the theory or other additional measurements. Here we consider the geometries which suppose to know only one phase difference.

Let’s consider two edge cases: (A) polarization of the second harmonic is along to propagation of fundamental one ( $\theta_a = 0$ ) (Figure 2a–c) and (B) polarization of the second harmonic is coplanar the plane of polarization of fundamental ( $\theta_a = \pi/2, \varphi_a = 0$ ) (Figure 2d–f).

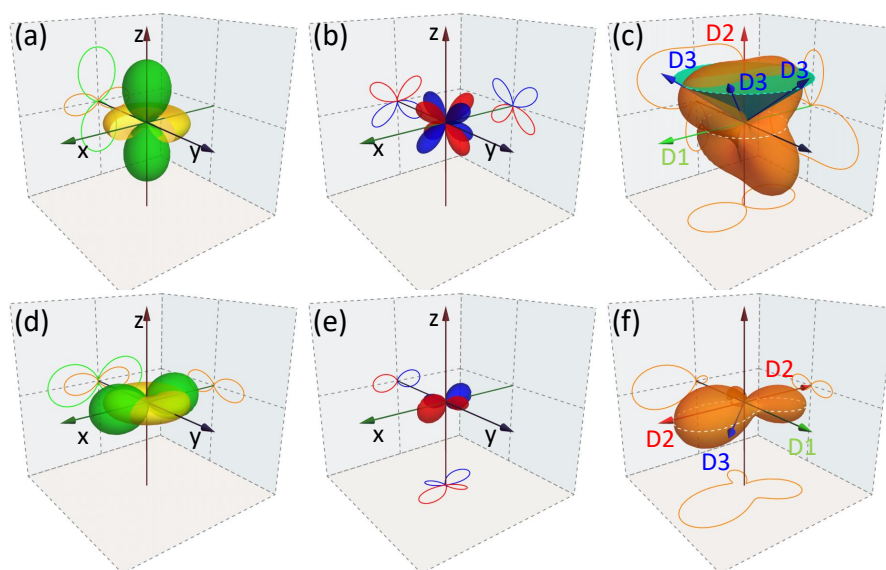


**Figure 2.** (a,d) Pattern of PAD caused by the incoherent one-photon (orange) and two-photon (green) ionization of a s-shell; (b,e) the contribution of the interference term, red color marks positive contribution, blue color—negative one; (c,f) the resulting PAD at bichromatic ionization. D1, D2 and D3 mark the suggested placement of the detectors (see text). (a–c) correspond to the geometry (A): linear polarization of  $2\omega$  is along to propagation direction of  $\omega$ ; (d–f) to the geometry (B): linear polarization of  $2\omega$  is in the plane of polarization  $\omega$ . The lines mark section of a presented contribution to PAD with corresponding coordinate plane.

In case (A) the incoherent sum of Equations (10) and (11) possesses an axial symmetry. Moreover, the photoelectron signal along the z-axis (detector D2) may be produced only by one-photon absorption and any signal in the xy-plane (detector D1) is due to the two-photon absorption. Therefore, two time-of-flight (ToF) detectors allow to eliminate both incoherent contributions (Figure 2b). Now let’s consider the plane formed by magic angle ( $\cos\vartheta = 1/\sqrt{3}$ ) where the expected interference is maximal. Because of the interference the signal of detector D3 oscillates with  $\phi$  around the averaged value  $4/9\text{signal}(D1) + 1/3\text{signal}(D2)$ . If one wants to extract the phase offset  $\phi$ , three detectors are needed. The best way to place detectors is to position them separated by  $\Delta\varphi = \pi/3$ , but, generally, three ToFs are enough at any position, except  $\varphi_1 = \varphi_2 + \pi$  where the emission signals are expected to be equal. If, as it happens in modern experiment [11,12,47], the phase offset  $\phi$  is changed, then one needs only one ToF detector at  $\vartheta = \arccos 1/\sqrt{3}$ , and PAD can be completely reconstructed from an oscillation of signal with  $\phi$ .

Two important features should be emphasized. First, if oscillation amplitude on detector D3 is lower than  $\frac{4}{3}\sqrt{\text{signal}(D1)\text{signal}(D2)}/3$ , then coherence is partly lost. Second,

there could be a fluctuation of harmonic intensities with phase offset (or energy) in an experiment. This fluctuation may be eliminated by appropriate scaling signals of 1st and 2nd detectors. Usually, another medium serves as a such monitor. For example, in recent paper [47] conjugate measurement of two gases, i.e., He and Ne, was applied to overcome this obstacle.

It is worth to be noted that the projection of the interference contribution Equation (12) onto any plane parallel to the z-axis is not eliminated that allows to use velocity map imaging (VMI) detectors. Positioning a VMI detector parallel to the xy-plane is hardly relevant because suggests that the fundamental harmonic irradiates it, but anyway the projection of the interference to this plane is zero i.e., interference contributions eliminate each other.

In case (B) the incoherent sum of Equations (10) and (11) possesses three symmetry planes (Figure 2d–f) formed by polarization of  $\omega$  (xy-plane), polarization of  $2\omega$  and propagation of  $\omega$  (xz-plane) and plane perpendicular to polarization of  $2\omega$  (yz-plane). Both probabilities of the one- and two-photon ionization as well as their interference (12) are maximal in the xy-plane, therefore positioning of ToFs in this plane is the most efficient. One ToF (D1) placed along the y-axis detects only the two-photon ionization by  $\omega$ , average signal of two ToFs placed with  $\delta\phi = \pi$  gives a probability of the one-photon ionization. As in case (A), there are two possibilities: three ToFs which allow to completely reconstruct the whole PAD or one ToF accompanying with changing phase offset  $\phi$ .

The interference term possesses six zeros: two of them are defined by the polarization vector of  $2\omega$  and four rotate with the phase offset between harmonics. Generally, a projection of PAD to a plane does not cancel the interference that allows to apply VMI detectors.

#### 4. Spectroscopy

In the limit of an infinitely long pulse the reduced transition amplitudes can be cast from the radial dipole matrix elements [52,53] as:

$$A_{\varepsilon p}^{(1)} = 2E_{2\omega} e^{i(\sigma_p - \phi)} \begin{cases} \int \psi_{\varepsilon p} r \psi_{1s} dr & \text{in length gauge} \\ -\int \psi_{\varepsilon p} (\frac{d}{dr} - \frac{1}{r}) \psi_{1s} dr & \text{in velocity gauge} \end{cases} \quad (13)$$

$$A_{\varepsilon s, \varepsilon d}^{(2)} = 2(10, 10 | 10) E_{\omega}^2 e^{i\sigma_{s,d}} \sum_n \frac{\int \psi_{1r} \psi_{n p} dr \int \psi_{n p} r \psi_{1s} dr}{\varepsilon_{1s} - \varepsilon_{sp} + \omega} \quad (14)$$

where  $\psi_{nl/el}$  are the bound/free radial wave functions and  $\sigma_{el}$  are phase shifts including both scattering and Coulomb phase; the factor “2” appears to consider filled s-shell, like the helium ground state. The summation in Equation (14) spans over all discrete and continuum states ( $s = n, \varepsilon'$ ) and can be done using variational approach described in [54,55]. Previously we successfully implemented and verified this method for H atom and He<sup>+</sup> ion in [56].

Let us briefly describe the method. According to it, the sum over  $n$  is separated as:

$$\int \psi_{\varepsilon s, \varepsilon d} \nu dr + \int \mu r \psi_{1s} dr + \int \mu (\varepsilon_{1s} + \omega - h(sp)) \nu dr \quad (15)$$

where  $\mu$  and  $\nu$  are the functions of special form that can be expressed as a finite sum of  $M$  Slater orbitals  $\Phi(m) = N_m r^m e^{-r}$ :

$$\mu = \sum_{m=1}^M a_m \Phi(m), \quad \nu = \sum_{m=1}^M b_m \Phi(m) \quad (16)$$

with  $N_m$  being the normalization constant and coefficients  $a_m$  and  $b_m$  obtained by solution of a system of  $2M$  linear algebraic equations:

$$\sum_{m=0}^M T_{nm} a_m = c_n, \quad \sum_{m=0}^M b_m T_{nm} = d_n \quad (17)$$

where

$$T_{nm} = \int \Phi(n)(\epsilon_{1s} + \omega - h(p))\Phi(m)dr, \tag{18}$$

$$h(p) = -\frac{1}{2} \frac{d^2}{dr^2} - \frac{V(r)}{r} + \frac{1}{r^2}, \tag{19}$$

$$c_n = \int \Phi(n)r\psi_{1s}dr, \quad d_m = \int \Phi(m)r\psi_{\epsilon s, \epsilon d}dr. \tag{20}$$

The single-electron wave functions were obtained by the RADIAL code [57] with MCHF [58] 2*p*-wave central potential  $V(r)$ . With such a potential the phase difference between *s*- and *d*-waves is in agreement with the measurements [59], while the accuracy of ground state is far from ideal: calculated ionization potential is  $-0.819$  a.u. versus experimental  $-0.904$  a.u.

In Figure 3, partial cross sections:

$$\sigma_{\epsilon p} = \frac{4\pi^2\omega}{3c} |A_{\epsilon p}^{(1)}|^2 \tag{21}$$

$$\sigma_{\epsilon s, \epsilon d}^{(2)} = \frac{2\pi\omega^2}{15F_0^2\tau_0} N |A_{\epsilon s, \epsilon d}^{(2)}|^2 \quad \begin{array}{l} \text{with } N = 5 \text{ for } s\text{-wave} \\ \text{and } N = 2 \text{ for } d\text{-wave} \end{array} \tag{22}$$

for one-photon (21) with  $\frac{4\pi^2\omega}{3c} = 2.69$  Mb (panel a) and two-photon (22) [52] with  $F_0 = 3.22 \times 10^{34} \text{ cm}^{-2}\text{s}^{-1}$  being an atomic unit of flux and  $\tau_0 = 2.42 \times 10^{-17} \text{ s}$  being an atomic unit of time ionization (panel b) are presented. The one-photon ionization cross section is compared with available experimental data [60]. We are not aware of any experiments on measuring sole two-photon ionization cross sections, but our results are in consistency with results obtained by other theoretical approaches [61–64]. Note that the ratio of amplitudes  $d_d/d_s$  ( $-\sqrt{5}A_0^{(2)}/\sqrt{4}A_2^{(2)}$ ) does not match the experimental results from ' $\omega + 2\omega$ ' measurements [12]: it seems that in real helium first minimum of  $d_s$  partial wave lies closer to the results obtained in [61] by a sophisticated B-spline R-matrix method.

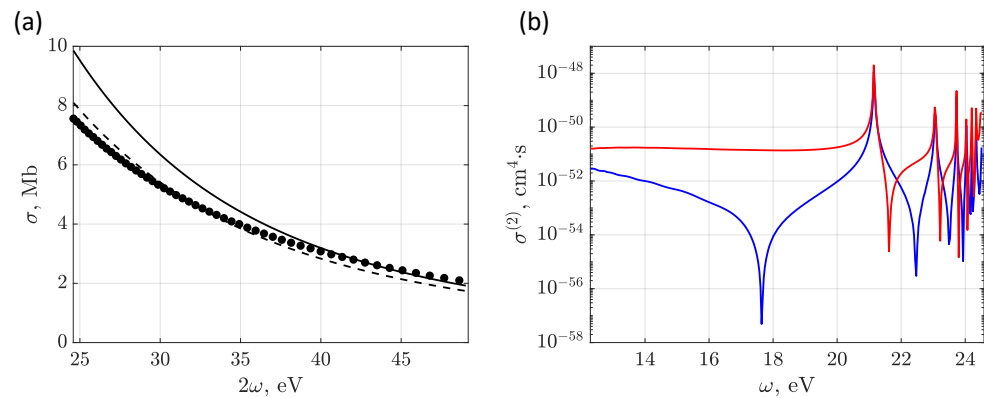


**Figure 3.** (a) One-photon cross section in length (solid line) and velocity (dashed) forms in comparison with experimental data [60] (dots); (b) Partial two-photon cross sections into *s*-wave (blue line) and *d*-wave (red) for linearly polarized radiation.

The analysis shown that  $M = 40$  is enough to reveal the lowest four resonances, while  $M = 60$  reproduces lowest six resonances. Their energies along with the experimental values are presented in Table 1.

An additional verification of our model can be retrieved from the analysis of the angular anisotropy parameters  $\beta_n$  for linearly polarized pulses. The  $\beta_2$  of the one-photon ionization from *s*-shell is geometrical and equals 2, the  $\beta_{2,4}$  of the two-photon ionization are calculated for a short pulses in [64], and, in general, are in consistency with our results.

**Table 1.** Calculated by the variationally stable method and experimental resonance energies.

Resonance	Theory	Experiment [65]
1s2p <sup>1P</sup>	21.14	21.22
1s3p <sup>1P</sup>	23.06	23.09
1s4p <sup>1P</sup>	23.73	23.74
1s5p <sup>1P</sup>	24.04	24.05
1s6p <sup>1P</sup>	24.21	24.21
1s7p <sup>1P</sup>	24.34	24.31

### 5. Results and Discussion

In this section we present and discuss an application of the developed approach to the ionization of helium ground state by the bichromatic field with fundamental harmonic  $20.0 \leq \omega \leq 24.5$  eV in order to trace the system behavior in the region of lowest excited states. In order to keep the discussion compact and avoid consideration of pulse duration and envelope effects which have been analyzed earlier [30,31], we consider an infinitely long pulse that can be characterized by two parameters: the ratio of fundamental and second harmonic electric strengths  $\eta = E_{2\omega}/E_\omega$  and their relative phase  $\phi$ .

Lets introduce a generalized parameter  $\mathcal{A}$  which determines the efficiency of the interference:

$$\mathcal{A} = \frac{\sqrt{\frac{3}{2}} |A_{\epsilon p}^{(1)} A_{\epsilon d}^{(2)*}|}{|A_{\epsilon p}^{(1)}|^2 + \frac{3}{8} |A_{\epsilon d}^{(2)}|^2}. \tag{23}$$

Note that a connection of the interference efficiency (23) with an asymmetry in any particular direction  $\{\theta, \varphi\}$  induced by the interference is not straightforward and curved by Equations (10)–(12).

In Figure 4a we present the asymmetry efficiency (23) as a function of fundamental energy  $\omega$  and the ratio of electric fields  $\eta$ . The interference between the one- and two-photon pathways is more pronounced when corresponding ionization probabilities are close. It is clearly seen that at resonance energies (see Table 1) a very high intensity of second harmonic is needed, whereas at minima of two-photon amplitude (Figure 3) the needed electrical strength drops by three orders of magnitude. However, this is true only for a infinity long pulses, and the real needed ratio in experiment is expected to be of one or two order of magnitudes lower at resonances and higher at minimas. The saw of maxima and minima contracts with energy becoming practically unresolved.

From Equation (12) one can see that a phase  $\phi$  providing the maximal asymmetry is defined by the phase difference in  $p$ - and  $d$ -channels, presented in Figure 4b. The scattering phases in helium are quite smooth in the region under consideration, and according to the basement of quantum mechanics, the two-photon amplitude exhibits a jump by  $\pi$  at resonances and at zeros.

In Figures 5a and 6a we present PADs at different phases between harmonics, for the geometries (A) and (B), correspondingly, accompanied with simulated detectors signals (Figures 5b and 6b).

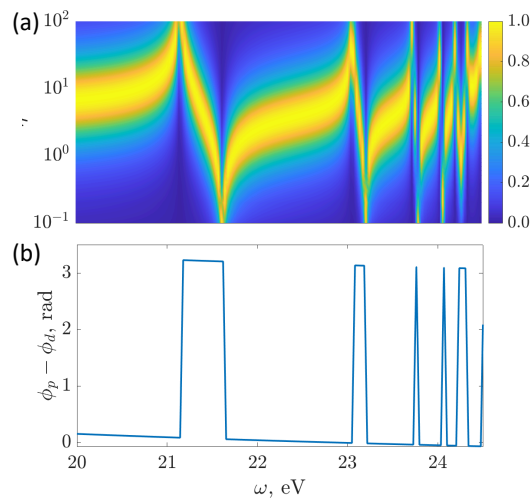


**Figure 4.** (a) The interference efficiency (23) as a function of fundamental energy and the harmonic strength ratio  $\eta = E_{2\omega}/E_\omega$ ; (b) The phase difference between  $p$  and  $d$  partial waves.

In Figure 5a PAD for the geometry (A) is sectioned with the  $xz$ -plane. While 3D PAD possesses two orthogonal planes of symmetry formed by  $\varphi = (\sigma_p - \sigma_d - \phi)/2$  and  $\varphi = (\sigma_p - \sigma_d - \phi)/2 + \pi/2$ , the section of this PAD with any plane containing  $z$ -axis is symmetrical with respect of it. For 3D PAD the symmetry with respect the  $xy$ -plane never takes place, but for the section it occurs at a condition  $\delta = \delta_p - \delta_d - \phi = \pi/2$  which occasionally (see Figure 4b) happens at  $\phi \approx \pi/2$  (violet line in Figure 5a).

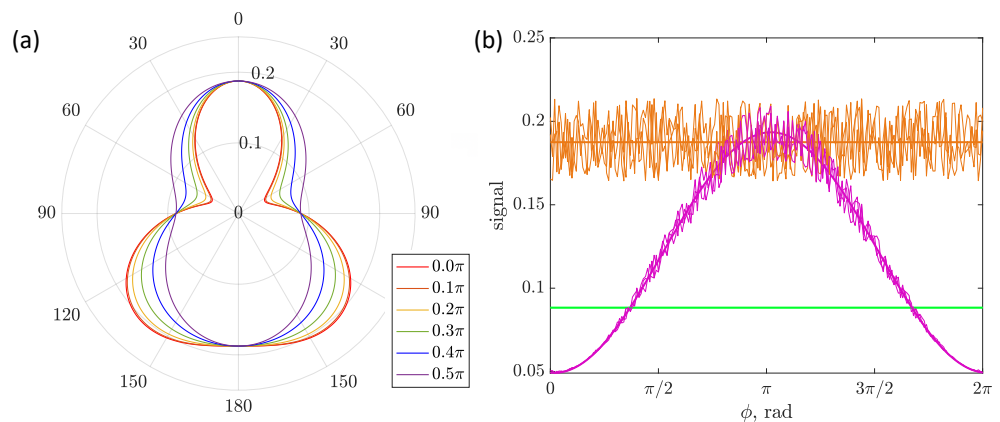


**Figure 5.** The photoemission signal at different phase shifts between the harmonics  $\phi$  for the geometry (A) at  $\omega = 21.55$  eV,  $\eta = 1$ . (a) PAD section with the  $xz$ -plane; (b) Signals of detector D1 (green line), D2 (orange line) and D3 (magenta line) assuming that there is a 25% strength fluctuation of the second harmonic with the phase  $\phi$ .

In Figure 6a PAD for the geometry (B) is sectioned with the  $xy$ -plane which is a plane of symmetry. All of the curves cross the same two points at the  $y$ -axis, indicating two zeros of Equation (12) independent of phase  $\phi$ . Obviously, incoherent sum of (10) and (11) does not depend on the phase. The sum of probabilities to be emitted along and opposite to  $x$ -axis does not depend on the phase. Additional symmetry planes of PAD ( $xz$  and  $yz$ ) arise when  $\delta = n\pi/2$ ,  $n \in \mathbb{Z}$  and in the considered system it is occasionally close to  $\phi = 0, \pi/2$  (red and violet lines in Figure 6a).

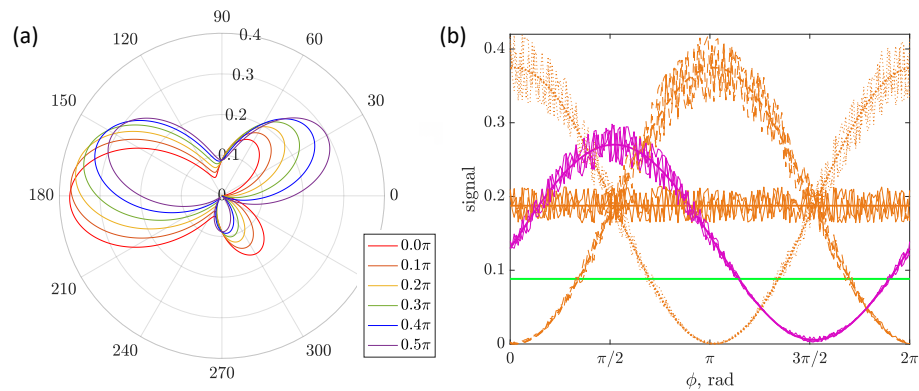


**Figure 6.** The photoemission signal at different phase shifts between the harmonics  $\phi$  for the geometry (B) at  $\omega = 21.55$  eV,  $\eta = 1$ . (a) PAD section with the  $xy$ -plane; (b) Signals of detector D1 (green line), D2 (orange lines, dotted and dashed for the two detectors separated by  $\pi$  and solid line for their average) and D3 (magenta line) assuming that there is a 25% strength fluctuation of the second harmonic with the phase  $\phi$ .

In Figures 5b and 6b we present simulated photoemission signal at detectors D1, D2 and D3 as a function of phase  $\phi$  assuming that the second harmonic emission suffers of a 25% fluctuation. For geometry (A) Figure 5b the detector D3 is placed  $\phi = 0$ , for geometry (B) D3 is placed  $\phi = \pi/4$ . One can see that even if there is a harmonic strength fluctuation, the detector D2 allows directly estimate it, and exclude this fluctuation from the interference part. An important finding never mentioned in connection with a bichromatic coherent control setup is that in the region where the interference is destructive, the fluctuations of the incoherent and coherent contributions cancel each other, while if interference is constructive, they are summed. If in an experiment there are very few points for oscillation (like we had in [47]), then upper part of oscillation can be completely distorted and should be treated as less reliable.

### 6. Complementary

In this section we present a possible extension of the above discussion. Equations (10)–(12) are easily generalized to the case of linearly polarized  $n$ -th harmonic  $n\omega$  ( $n$  must be even) accompanied with circularly polarized fundamental harmonic of frequency  $\omega$ :

$$W^\omega(\vartheta, \varphi) = \frac{1}{4\pi} |A_{\varepsilon n}^{(n)}|^2 \cdot \frac{(2n-1)!!}{2^n n!} \sin^{2n} \vartheta; \tag{24}$$

the contribution of single-photon ionization by linearly polarized  $n$ -th harmonic:

$$W^{n\omega}(\vartheta, \varphi) = \frac{1}{4\pi} |A_{\varepsilon p}^{(1)}|^2 (\cos \theta_a \cos(\vartheta) + \sin \theta_a \sin \vartheta \cos(\phi_p - \varphi))^2; \tag{25}$$

and, finally, the interference term:

$$W^{(\omega, n\omega)}(\vartheta, \varphi) = \frac{1}{4\pi} |A_{\varepsilon p}^{(1)} A_{\varepsilon n}^{(n)*}| \frac{\sqrt{(2n-1)!!}}{2^{(n/2-1)} \sqrt{n!}} \sin^n \vartheta \cos(n\varphi - \delta) (\cos(\theta_a) \cos(\vartheta) + \sin \theta_a \sin \vartheta \cos(\phi_p - \varphi)). \tag{26}$$

The condition that  $n$  is even means that the interference of  $n$ -photon and one-photon amplitudes manifests in angular dependency only (26), what differs from the case  $\omega = 3\omega$  considered in [66]. The general discussion remains the same with two differences: (1) for the geometry (A) there is  $n$  symmetry planes containing  $z$ -axis and separated by the angle  $2\pi/n$  instead of two orthogonal planes (see Section 2); (2) for the geometry (B) there are two zeros of the interference which are steady and  $2(n-1)$  zeros which rotates at phase changing. The cases either  $n$  is even or  $n$  odd (considered for example in [66]) differ due to

fact that the electrons ionized by the absorption of odd and even number of photons have opposite parities. Therefore, in the case of an even  $n$ , the interference term (25) has an odd rank of an angular dependency, and in the case of an odd  $n$ , it is of an even rank. Therefore in the second case the meaning of “asymmetry” (23) is more difficult to interpret.

## 7. Conclusions

In the paper we consider those exclusive geometries, i.e., polarization and mutual orientation of harmonics, which allow to access the phase offset between them with minimal number of the theoretical (spectroscopic) assumptions. In an ideal case only one parameter, namely a phase between two ionization channels, is needed. These geometries allow to (a) access the phase between harmonics, (b) directly without any theoretical assumption get the contributions of the single- and two-photon ionization, (c) estimate degree of coherency between the harmonics, and (d) exclude an occasional fluctuation of the harmonic intensities.

Additionally, we found that in the bichromatic coherent control setup a lower part of oscillation is more stable in case of a fluctuation than an upper part, and should be treated at fitting as more reliable.

We believe that the presented research can pave the way to future experiments.

**Author Contributions:** Conceptualization, E.V.G. and A.N.G.-G.; methodology, M.M.P.; software, M.M.P.; validation, E.V.G. and M.M.P.; writing—original draft preparation, E.V.G. and M.M.P.; writing—review and editing, E.V.G., M.M.P. and A.N.G.-G.; visualization, E.V.G. and M.M.P.; supervision, A.N.G.-G. All authors have read and agreed to the published version of the manuscript.

**Funding:** This research was funded by RSF grant number 22-12-00389.

**Institutional Review Board Statement:** Not applicable.

**Informed Consent Statement:** Not applicable.

**Data Availability Statement:** Data sharing not applicable.

**Conflicts of Interest:** The authors declare no conflict of interest.

## References

1. Goepfert-Mayer, M. Uber Elementarakte mit zwei Quantensprungen (Elementary processes with two quantum transitions). *Ann. Phys.* **1951**, *9*, 273. (In German)
2. Kohler, M.; Pfeifer, T.; Hatsagortsyan, K.; Keitel, C. Chapter 4—Frontiers of Atomic High-Harmonic Generation. In *Advances in Atomic, Molecular, and Optical Physics*; Berman, P., Arimondo, E., Lin, C., Eds.; Academic Press: Cambridge, MA, USA, 2012; Volume 61, pp. 159–208. [[CrossRef](#)]
3. Krausz, F.; Ivanov, M. Attosecond physics. *Rev. Mod. Phys.* **2009**, *81*, 163–234. [[CrossRef](#)]
4. Strelkov, V.V.; Platonenko, V.T.; Sterzhantov, A.F.; Ryabikin, M.Y. Attosecond electromagnetic pulses: generation, measurement, and application. Generation of high-order harmonics of intense laser field for attosecond pulse production. *Phys. Usp.* **2016**, *59*, 425. [[CrossRef](#)]
5. Allaria, E.; Appio, R.; Badano, L.; Barletta, W.A.; Bassanese, S.; Biedron, S.G.; Borga, A.; Busetto, E.; Castronovo, D.; Cinquegrana, P.; et al. Highly Coherent Stable Pulses FERMI Seeded Free-Electron Laser Extrem Ultraviolet. *Nat. Photonics* **2012**, *6*, 699. [[CrossRef](#)]
6. Callegari, C.; Grum-Grzhimailo, A.N.; Ishikawa, K.L.; Prince, K.C.; Sansone, G.; Ueda, K. Atomic, molecular and optical physics applications of longitudinally coherent and narrow bandwidth Free-Electron Lasers. *Phys. Rep.* **2021**, *904*, 1–59. [[CrossRef](#)]
7. Prince, K.C.; Allaria, E.; Callegari, C.; Cucini, R.; Ninno, G.D.; Mitri, S.D.; Diviacco, B.; Ferrari, E.; Finetti, P.; Gauthier, D.; et al. Coherent control with a short-wavelength free-electron laser. *Nat. Photonics* **2016**, *10*, 176–179. [[CrossRef](#)]
8. Paul, P.M.; Toma, E.S.; Breger, P.; Mullot, G.; Augé, F.; Balcou, P.; Muller, H.G.; Agostini, P. Observation of a Train of Attosecond Pulses from High Harmonic Generation. *Science* **2001**, *292*, 1689–1692. [[CrossRef](#)] [[PubMed](#)]
9. Tzallas, P.; Charalambidis, D.; Papadogiannis, N.A.; Witte, K.; Tsakiris, G.D. Direct observation of attosecond light bunching. *Nature* **2003**, *426*, 267–271. [[CrossRef](#)]
10. Maroju, P.K.; Grazioli, C.; Di Fraia, M.; Moioli, M.; Ertel, D.; Ahmadi, H.; Plekan, O.; Finetti, P.; Allaria, E.; Giannessi, L. Attosecond pulse shaping using a seeded free-electron laser. *Nature* **2020**, *578*, 386–391. [[CrossRef](#)]
11. You, D.; Ueda, K.; Gryzlova, E.V.; Grum-Grzhimailo, A.N.; Popova, M.M.; Staroselskaya, E.I.; Tugs, O.; Orimo, Y.; Sato, T.; Ishikawa, K.L.; et al. New Method for Measuring Angle-Resolved Phases in Photoemission. *Phys. Rev. X* **2020**, *10*, 031070. [[CrossRef](#)]

12. Di Fraia, M.; Plekan, O.; Callegari, C.; Prince, K.C.; Giannessi, L.; Allaria, E.; Badano, L.; De Ninno, G.; Trovò, M.; Diviacco, B.; et al. Complete Characterization of Phase and Amplitude of Bichromatic Extreme Ultraviolet Light. *Phys. Rev. Lett.* **2019**, *123*, 213904. [[CrossRef](#)] [[PubMed](#)]
13. Armstrong, G.S.J.; Clarke, D.D.A.; Benda, J.; Wragg, J.; Brown, A.C.; van der Hart, H.W. Modeling tomographic measurements of photoelectron vortices in counter-rotating circularly polarized laser pulses. *Phys. Rev. A* **2019**, *100*, 063416. [[CrossRef](#)]
14. Niikura, H.; Dudovich, N.; Villeneuve, D.M.; Corkum, P.B. Mapping Molecular Orbital Symmetry on High-Order Harmonic Generation Spectrum Using Two-Color Laser Fields. *Phys. Rev. Lett.* **2010**, *105*, 053003. [[CrossRef](#)] [[PubMed](#)]
15. Sarantseva, T.S.; Frolov, M.V.; Manakov, N.L.; Ivanov, M.Y.; Starace, A.F. Harmonic generation spectroscopy with a two-colour laser field having orthogonal linear polarizations. *J. Phys. B At. Mol. Opt. Phys.* **2013**, *46*, 231001. [[CrossRef](#)]
16. Milošević, D.B.; Becker, W.; Kopold, R. Generation of circularly polarized high-order harmonics by two-color coplanar field mixing. *Phys. Rev. A* **2000**, *61*, 063403. [[CrossRef](#)]
17. Fleischer, A.; Kfir, O.; Diskin, T.; Sidorenko, P.; Cohen, O. Spin angular momentum and tunable polarization in high-harmonic generation. *Nat. Photonics* **2014**, *8*, 543–549. [[CrossRef](#)]
18. Chen, C.; Tao, Z.; Hernández-García, C.; Matyba, P.; Carr, A.; Knut, R.; Kfir, O.; Zusin, D.; Gentry, C.; Grychtol, P.; et al. Tomographic reconstruction of circularly polarized high-harmonic fields: 3D attosecond metrology. *Sci. Adv.* **2016**, *2*, e1501333. [[CrossRef](#)]
19. Khairulin, I.; Antonov, V.; Ryabikin, M.; Berrill, M.A.; Shlyaptsev, V.N.; Rocca, J.J.; Kocharovskaya, O. Amplification of elliptically polarized sub-femtosecond pulses in neon-like X-ray laser modulated by an IR field. *Sci. Rep.* **2022**, *12*, 6204. [[CrossRef](#)]
20. Demekhin, P.V.; Artemyev, A.N.; Kastner, A.; Baumert, T. Photoelectron Circular Dichroism with Two Overlapping Laser Pulses of Carrier Frequencies  $\omega$  and  $2\omega$  Linearly Polarized in Two Mutually Orthogonal Directions. *Phys. Rev. Lett.* **2018**, *121*, 253201. [[CrossRef](#)]
21. Mayer, N.; Patchkovskii, S.; Morales, F.; Ivanov, M.; Smirnova, O. Imprinting Chirality on Atoms Using Synthetic Chiral Light Fields. *Phys. Rev. Lett.* **2022**, *129*, 243201. [[CrossRef](#)]
22. De Silva, A.H.N.C.; Atri-Schuller, D.; Dubey, S.; Acharya, B.P.; Romans, K.L.; Foster, K.; Russ, O.; Compton, K.; Rischbieter, C.; Douguet, N.; et al. Using Circular Dichroism to Control Energy Transfer in Multiphoton Ionization. *Phys. Rev. Lett.* **2021**, *126*, 023201. [[CrossRef](#)]
23. Zipp, L.J.; Natan, A.; Bucksbaum, P.H. Probing electron delays in above-threshold ionization. *Optica* **2014**, *1*, 361–364. [[CrossRef](#)]
24. Cao, C.; Li, M.; Liang, J.; Yan, J.; Guo, K.; Li, Z.; Liu, Y.; Zhou, Y.; Lu, P. Angular distribution of near-threshold photoelectrons from resonance-enhanced multiphoton ionization of argon. *Phys. Rev. A* **2022**, *106*, 033112. [[CrossRef](#)]
25. López, S.D.; Donsa, S.; Nagele, S.; Arbó, D.G.; Burgdörfer, J. Phase delays in  $\omega - 2\omega$  above-threshold ionization. *Phys. Rev. A* **2021**, *104*, 043113. [[CrossRef](#)]
26. Ayuso, D.; Jiménez-Galán, A.; Morales, F.; Ivanov, M.; Smirnova, O. Attosecond control of spin polarization in electron-ion recollision driven by intense tailored fields. *New J. Phys.* **2017**, *19*, 073007. [[CrossRef](#)]
27. Milošević, D.B. Atomic and Molecular Processes in a Strong Bicircular Laser Field. *Atoms* **2018**, *6*, 61. [[CrossRef](#)]
28. Schafer, K.J.; Kulander, K.C. Phase-dependent effects in multiphoton ionization induced by a laser field and its second harmonic. *Phys. Rev. A* **1992**, *45*, 8026–8033. [[CrossRef](#)] [[PubMed](#)]
29. Douguet, N.; Bartschat, K. Photoelectron momentum distributions in the strong-field ionization of atomic hydrogen by few-cycle elliptically polarized optical pulses. *Phys. Rev. A* **2022**, *106*, 053112. [[CrossRef](#)]
30. Grum-Grzhimailo, A.N.; Gryzlova, E.V.; Staroselskaya, E.I.; Venzke, J.; Bartschat, K. Interfering one-photon and two-photon ionization by femtosecond VUV pulses in the region of an intermediate resonance. *Phys. Rev. A* **2015**, *91*, 063418. [[CrossRef](#)]
31. Gryzlova, E.V.; Grum-Grzhimailo, A.N.; Staroselskaya, E.I.; Douguet, N.; Bartschat, K. Quantum coherent control of the photoelectron angular distribution in bichromatic-field ionization of atomic neon. *Phys. Rev. A* **2018**, *97*, 013420. [[CrossRef](#)]
32. Baranova, N.B.; Beterov, I.M.; Zel'dovich, B.Y.; Ryabtsev, I.I.; Chudinov, A.N.; Shul'ginov, A.A. Observation of an interference of one- and two-photon ionization of the sodium 4s state. *Pis'ma Zh. Eksp. Teor. Fiz.* **1992**, *55*, 431. (*JETP Lett.* **1992**, *55*, 439)
33. Anderson, D.Z.; Baranova, N.B.; Green, K.; Zel'dovich, B.Y. Interference of one- and two-photon processes in the ionization of atoms and molecules. *Zh. Eksp. Teor. Fiz.* **1992**, *75*, 210. (*JETP Lett.* **1992**, *102*, 397)
34. Yin, Y.Y.; Chen, C.; Elliott, D.S.; Smith, A.V. Asymmetric photoelectron angular distributions from interfering photoionization processes. *Phys. Rev. Lett.* **1992**, *69*, 2353–2356. [[CrossRef](#)] [[PubMed](#)]
35. Ehlotzky, F. Atomic phenomena in bichromatic laser fields. *Phys. Rep.* **2001**, *345*, 175–264. [[CrossRef](#)]
36. Shapiro, M.; Brumer, P. Coherent Control of Atomic, Molecular, and Electronic Processes. In *Advances in Atomic, Molecular, and Optical Physics*; Academic Press: Cambridge, MA, USA, 2000; Volume 42, pp. 287–345. [[CrossRef](#)]
37. Ohmura, H.; Nakanaga, T.; Tachiya, M. Coherent Control of Photofragment Separation in the Dissociative Ionization of IBr. *Phys. Rev. Lett.* **2004**, *92*, 113002. [[CrossRef](#)]
38. Goetz, R.E.; Koch, C.P.; Greenman, L. Quantum Control of Photoelectron Circular Dichroism. *Phys. Rev. Lett.* **2019**, *122*, 013204. [[CrossRef](#)]
39. Stevens, M.J.; Smirl, A.L.; Bhat, R.D.R.; Najmaie, A.; Sipe, J.E.; van Driel, H.M. Quantum Interference Control of Ballistic Pure Spin Currents in Semiconductors. *Phys. Rev. Lett.* **2003**, *90*, 136603. [[CrossRef](#)]
40. Fortier, T.M.; Roos, P.A.; Jones, D.J.; Cundiff, S.T.; Bhat, R.D.R.; Sipe, J.E. Carrier-Envelope Phase-Controlled Quantum Interference of Injected Photocurrents in Semiconductors. *Phys. Rev. Lett.* **2004**, *92*, 147403. [[CrossRef](#)]

41. Popova, M.M.; Gryzlova, E.V.; Kiselev, M.D.; Grum-Grzhimailo, A.N. Symmetry Violation in Bichromatic Ionization by a Free-Electron Laser: Photoelectron Angular Distribution and Spin Polarization. *Symmetry* **2021**, *13*, 1015. [CrossRef]
42. Manakov, N.L.; Ovsianikov, V.D.; Starace, A.F. dc Field-Induced, Phase and Polarization Control of Interference between One- and Two-Photon Ionization Amplitudes. *Phys. Rev. Lett.* **1999**, *82*, 4791–4794. [CrossRef]
43. Bolovinos, A.; Cohen, S.; Lontos, I. One- and two-photon phase-sensitive coherent control of total ionization yields in the presence of static electric fields. *Phys. Rev. A* **2008**, *77*, 023413. [CrossRef]
44. Yamazaki, R.; Elliott, D.S. Strong variation of the phase lag in the vicinity of autoionizing resonances. *Phys. Rev. A* **2007**, *76*, 053401. [CrossRef]
45. Bello, R.Y.; Borràs, V.J.; González-Vázquez, J.; Martín, F. Electronic coherences in argon through interfering one- and two-photon ionization processes in the vicinity of Feshbach resonances. *Phys. Rev. Res.* **2022**, *4*, 043028. [CrossRef]
46. Wang, Y.; Greene, C.H. Coherent-control phase lag across doubly excited atomic strontium resonances in an  $\omega - 2\omega$  interference scheme. *Phys. Rev. A* **2023**, *107*, 032804. [CrossRef]
47. Gryzlova, E.V.; Carpeggiani, P.; Popova, M.M.; Kiselev, M.D.; Douguet, N.; Reduzzi, M.; Negro, M.; Comby, A.; Ahmadi, H.; Wanie, V.; et al. Influence of an atomic resonance on the coherent control of the photoionization process. *Phys. Rev. Res.* **2022**, *4*, 033231. [CrossRef]
48. Hofbrucker, J.; Böning, B.; Volotka, A.V.; Fritzsche, S. Elliptical dichroism in biharmonic ionization of atoms. *Phys. Rev. A* **2021**, *104*, 013102. [CrossRef]
49. Fritzsche, S.; Hofbrucker, J. Biharmonic ( $\omega, 2\omega$ ) ionization of atoms by elliptically-polarized light. Carving the photoelectron angular distributions. *New J. Phys.* **2022**, *24*, 103031. [CrossRef]
50. Popova, M.M.; Gryzlova, E.V.; Kiseleva, M.D.; Grum-Grzhimailo, A.N. Ionization of Atoms by a Bichromatic Fields of  $\omega + 2\omega$  Multiple Frequencies with Arbitrary Polarization. *J. Exp. Theor. Phys.* **2022**, *135*, 58–72. [CrossRef]
51. Balashov, V.V.; Grum-Grzhimailo, A.N.; Kabachnik, M. *Polarization and Correlation Phenomena in Atomic Collisions. A Practical Theory Course*; Kluwer Plenum: New York, NY, USA, 2000. [CrossRef]
52. Cormier, E.; Lambropoulos, P. Extrapolation method for the evaluation of above threshold ionization cross sections for one- and two-electron systems. *J. Phys. B At. Mol. Opt. Phys.* **1995**, *28*, 5043. [CrossRef]
53. Sobelman, I.I. *Atomic Spectra and Radiative Transitions*; Springer: Berlin/Heidelberg, Germany, 1992. [CrossRef]
54. Gao, B.; Starace, A.F. Variational Calculation of Multiphoton Ionization Processes for the H Atom. *Phys. Rev. Lett.* **1988**, *61*, 404–407. [CrossRef]
55. Orel, A.; Rescigno, T. An algebraic variational approach to the calculation of total cross sections for one- and two-photon ionization. *Chem. Phys. Lett.* **1988**, *146*, 434–438. [CrossRef]
56. Staroselskaya, E.; Grum-Grzhimailo, A. A variationally stable method in the problem of two-photon atomic ionization. *Mosc. Univ. Phys. Bull.* **2015**, *70*, 374–381. [CrossRef]
57. Salvat, F.; Fernández-Varea, J.M. radial: A Fortran subroutine package for the solution of the radial Schrödinger and Dirac wave equations. *Comput. Phys. Commun.* **2019**, *240*, 165–177. [CrossRef]
58. Froese Fischer, C.; Brage, T.; Jönsson, P. *Computational Atomic Structure. An MCHF Approach*; Institute of Physics Publishing: Bristol, UK, 1997. [CrossRef]
59. Haber, L.H.; Doughty, B.; Leone, S.R. Continuum phase shifts and partial cross sections for photoionization from excited states of atomic helium measured by high-order harmonic optical pump-probe velocity map imaging. *Phys. Rev. A* **2009**, *79*, 031401. [CrossRef]
60. Marr, G.; West, J. Absolute photoionization cross-section tables for helium, neon, argon, and krypton in the VUV spectral regions. *At. Data Nucl. Data Tables* **1976**, *18*, 497–508. [CrossRef]
61. Saenz, A.; Lambropoulos, P. Theoretical two-, three- and four-photon ionization cross sections of helium in the XUV range. *J. Phys. B At. Mol. Opt. Phys.* **1999**, *32*, 5629. [CrossRef]
62. Nikolopoulos, L.A.A.; Lambropoulos, P. Multichannel theory of two-photon single and double ionization of helium. *J. Phys. B At. Mol. Opt. Phys.* **2001**, *34*, 545. [CrossRef]
63. Hofbrucker, J.; Volotka, A.V.; Fritzsche, S. Maximum Elliptical Dichroism in Atomic Two-Photon Ionization. *Phys. Rev. Lett.* **2018**, *121*, 053401. [CrossRef]
64. Boll, D.I.R.; Fojón, O.A.; McCurdy, C.W.; Palacios, A. Angularly resolved two-photon above-threshold ionization of helium. *Phys. Rev. A* **2019**, *99*, 023416. [CrossRef]
65. Kramida, A.; Ralchenko, Y.; Reader, J.; NIST ASD Team. *NIST Atomic Spectra Database (Ver. 5.10)*; National Institute of Standards and Technology: Gaithersburg, MD, USA, 2022. Available online: <https://physics.nist.gov/asd> (accessed on 24 July 2023).
66. Hofbrucker, J.; Ramakrishna, S.; Volotka, A.V.; Fritzsche, S. Polarization effects in the total rate of biharmonic  $\omega + 3\omega$  ionization of atoms. *Phys. Rev. A* **2022**, *106*, 013118. [CrossRef]

**Disclaimer/Publisher's Note:** The statements, opinions and data contained in all publications are solely those of the individual author(s) and contributor(s) and not of MDPI and/or the editor(s). MDPI and/or the editor(s) disclaim responsibility for any injury to people or property resulting from any ideas, methods, instructions or products referred to in the content.